12-2013

Kinematic Synthesis of Planar, Shape-Changing, Rigid Body Mechanisms for Design Profiles with Significant Differences in Arc Length

Shamsul A. Shamsudin
Universiti Teknikal

Andrew P. Murray
University of Dayton, amurray1@udayton.edu

David H. Myszka
University of Dayton, dmyszka1@udayton.edu

James P. Schmiedeler
University of Notre Dame

Kinematic Synthesis of Planar, Shape-Changing Rigid Body Mechanisms for Design Profiles with Significant Differences in Arc Length

Shamsul A. Shamsudin[a], Andrew P. Murray[a], David H. Myszka[a,*], James P. Schmiedeler[b]

[a]*Department of Mechanical and Aerospace Engineering, University of Dayton, Dayton, OH, 45469, USA.*
[b]*Department of Aerospace and Mechanical Engineering, University of Notre Dame, Notre Dame, IN, 46556, USA.*

Abstract

This paper presents a kinematic procedure to synthesize planar mechanisms capable of approximating a shape change defined by a general set of curves. These "morphing curves," referred to as design profiles, differ from each other by a combination of displacement in the plane, shape variation, and notable differences in arc length. Where previous rigid-body shape-change work focused on mechanisms composed of rigid links and revolute joints to approximate curves of roughly equal arc length, this work introduces prismatic joints into the mechanisms in order to produce the different desired arc lengths. A method is presented to iteratively search along the profiles for locations that are best suited for prismatic joints. The result of this methodology is the creation of a chain of rigid bodies connected by revolute and prismatic joints that can approximate a set of design profiles.

Keywords: Similarity transformation, image registration, rigid body mechanisms, shape-change, prismatic joints.

1. Introduction

The focus of much study has been on shape morphing aircraft wings that increase performance over a range of flight conditions [1, 2], and most of the design work has centered on changing between wing profiles of similar arc length [3, 4, 5]. The fundamentals of aerodynamics suggest, however, that lift and drag can be significantly altered with a change in camber and chord [6]. That is, for high lift situations (e.g., approach, landing, and climb), a higher camber and longer absolute chord are desirable, whereas for efficient cruising, a lower camber and shorter chord are desirable.

Many other mechanical systems benefit from the capacity to vary between specific shapes in a controlled manner. In addition to airfoils, shape changing systems have been used in other flow-field applications such as active boat hulls [7]. Advances in electro-optics resulting from shape change include active aperture antennas [8] and deformable mirrors [9]. Automotive convertible roofs [10] and portable performance stages [11] involve shape changes in structural applications. In manufacturing, robotic grippers [12] are designed to move between prescribed shapes. Altering an

*Corresponding author: Tel: +001 937-229-2968 Fax: +001 937-229-4766
Email addresses: shamsudins1@udayton.edu (Shamsul A. Shamsudin), amurray1@dayton.edu (Andrew P. Murray), dmyszka@dayton.edu (David H. Myszka), schmiedeler.4@edu (James P. Schmiedeler)

extruded plastic profile by sliding segments of the die orifice in a controlled manner [13] may also be considered shape change. As with airfoils, many of these example application areas could have optimal designs that require relaxation of the constraint that the various morphing shapes all be of identical arc length.

Shape change may be accomplished by using compliant mechanisms, which can be designed in manner similar to rigid-body mechanisms [14]. Without hinges, though, compliant mechanisms have the advantage of providing a smooth morphing boundary without discontinuities. Lu and Kota [15] used optimization algorithms to search discrete characteristics of a topology to best utilize compliant mechanisms to control the change of shape of a parabolic antenna. Moon [16] used compliant mechanisms to approximate the shape of a human finger during gripping motion, and Mohd Zubir et al. [22] similarly used a compliant mechanism for a microgripper. Limaye et al. [17] incorporated compliant kits of beams and connectors to generate a morphing aircraft wing. The displacement achievable with a compliant mechanism, however, is limited by the elastic properties of its composing material, so it is quite difficult to accommodate shape changes involving significant differences in arc length with a compliant mechanism.

For shape changes accomplished with rigid-body mechanisms, the edge geometries of some links are chosen to approximate a set of specific shapes [18]. A formalized process for creating such rigid-body shape-change mechanisms has been developed for shapes, called design profiles, characterized by open curves [19], closed curves [20], and curves with fixed endpoints [21]. In all cases, the prescribed profiles are constrained to have nearly constant arc length. The developments presented in this paper enable a chain of rigid bodies to approximate design profiles that exhibit significant differences in arc length.

The general process of rigid-body, shape-changing mechanism design is as follows. The problem is posed by specifying a set of design profiles, such as airfoil profiles for loiter and attack modes. The synthesis process begins by representing each of the design profiles in a standardized manner such that comparisons can be made among them. This standardized representation is a coordinated set of points on the design profile defining a piecewise curve that is called the target profile. The design process continues with a segmentation phase that creates segments, which are generated in shape and length so that they form rigid links that approximate corresponding portions on each target profile. To complete the synthesis, a mechanization phase adds binary links to each segment in order to achieve a lower degree-of-freedom (DOF) linkage. A system with fewer DOF is commonly preferred for simplicity in control [23, 24]. Although this general process of designing a rigid-body, shape-changing mechanism remains true for this work, substantial changes are needed to allow for significant differences in arc length.

Target profiles were originally defined in [19] such that all contained the same number of points. This definition is fundamentally lacking for profiles of different arc lengths because the large variations in the distance between consecutive points complicates the comparison of profile shapes. To properly compare various length profiles, the target profile definition was changed to produce a nearly constant distance between consecutive points on each profile, resulting in a different number of points on each. During the segmentation phase, the constant arc length segment was preserved from the preceding methodology. Necessitated by various arc lengths, however, a new type of segment has been developed that includes a prismatic joint allowing the segment to change length in matching the set of design

profiles. Additionally, the prior segmentation methodology has been transformed to iteratively search for locations along the profiles best suited for the prismatic joints. Lastly, a new process is outlined to detect revolute joints exhibiting minimal motion and combine the adjoining segments as to reduce mechanism complexity. Combining the two types of segments in this fashion introduces a third, compound segment type.

The remainder of the paper is organized as follows. Section 2 addresses a new process for converting design profiles into target profiles having similar spacing between defining points. Section 3 presents a process for segmenting regions along target profiles that will form the rigid bodies. Section 4 discusses the process for assessing the segmentation error and a method for adjusting the segments to improve profile matching. Section 5 presents the method to join the chain with revolute joints, and Section 6 discusses a process to merge segments when the associated revolute joint exhibits minimal rotation. Section 7 reviews mechanization and examples are given in Section 8.

2. Design and Target Profiles

The shape-change problem is posed by specifying a set of p design profiles that represent the different shapes to be attained by the mechanism. Murray et al. [19] define a design profile j as an ordered set of N_j points for which the arc length between any two can be determined. Figure 1 shows the three types of design profiles considered: open, closed, and fixed-end profiles. While the illustrative examples shown in this paper are for the open profile case, this research establishes a process to form a chain of rigid links to approximate any of these types of profiles.

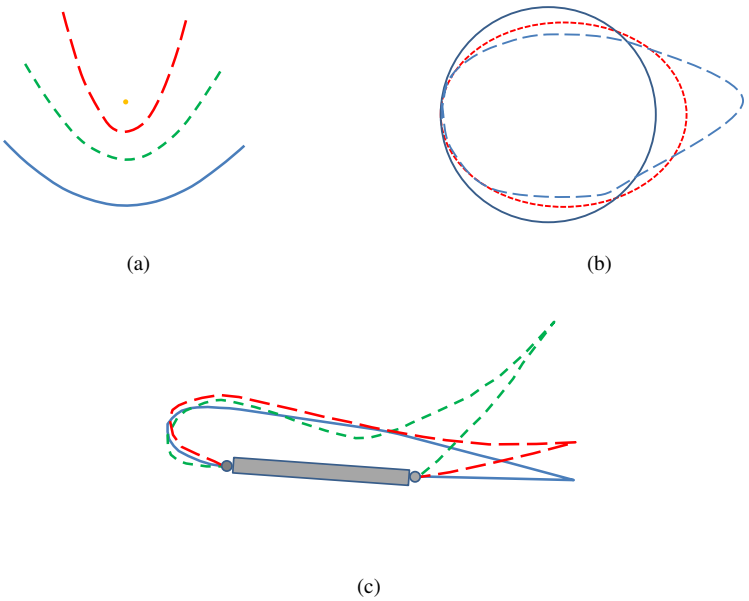

Figure 1: Types of design profiles include (a) open profiles, (b) closed profiles, and (c) fixed-end profiles.

Given the definition of design profiles, they may be viewed as being piecewise linear [25, 26]. A piece is the line

segment connecting two contiguous points on a profile. The i^{th} point on the j^{th} design profile is designated $\left\{a_{j_i}, b_{j_i}\right\}^T$. The length of the i^{th} piece on the j^{th} design profile is

$$c_{j_i} = \sqrt{\left(a_{j_{i+1}} - a_{j_i}\right)^2 + \left(b_{j_{i+1}} - b_{j_i}\right)^2}, \tag{1}$$

and the arc length of the entire j^{th} design profile is

$$C_j = \sum_{i=1}^{N_j - 1} c_{j_i}. \tag{2}$$

The design profiles may be defined by any number of points spaced at various intervals, producing a wide range of c_{j_i}.

Target profiles are a set of curves that represent the set of design profiles. They have common features so that groups of contiguous points can be compared among all profiles in order to form a suitable chain of rigid bodies that when repositioned will approximate all design profiles. In earlier work [19, 20], the design profiles were assumed to be of roughly equal arc lengths, $C_1 \approx C_2 \approx \ldots \approx C_p$. In that case, each target profile can be formed by distributing the same n number of defining points equally along the corresponding design profile. The target profile becomes a piecewise linear curve composed of pieces with roughly the same length, $c_{j_i} \approx c_{k_l}$, $\forall\, i, j, k, l$. Constant piece lengths allow for identification of corresponding points on each target profile.

The general profiles discussed in this paper may possess large differences in arc length. Using the same number of points on different length profiles would result in different piece lengths and contaminate the shape comparisons among groupings of contiguous points. In order to produce a constant piece length, the conversion scheme from design to target profiles must be modified to allow for a different number of points on each target profile. By specifying a desired piece length s_d, the number of pieces m_j on profile j can be determined. Smaller values of s_d will produce more pieces and typically result in smaller variations between the design and target profiles.

The number of pieces must be an integer, and an initial value is calculated as

$$m_j = \left\lceil \frac{C_j}{s_d} \right\rceil, \tag{3}$$

where $\lceil \zeta \rceil$ represents the ceiling function, the smallest integer not less than ζ. Provisional target profiles are generated by distributing n_j points at increments of C_j/m_j along the j^{th} design profile. A distribution of target profile points along a design profile is shown in Fig. 2. The j^{th} target profile becomes a piecewise linear curve connecting the ordered set of points $\mathbf{z}_{j_i} = \left\{x_{j_i}, y_{j_i}\right\}^T$, $i = 1, ..., n_j$. The length of the i^{th} linear piece on the j^{th} target profile is

$$s_{j_i} = \left\|\mathbf{z}_{j_{i+1}} - \mathbf{z}_{j_i}\right\| = \sqrt{\left(x_{j_{i+1}} - x_{j_i}\right)^2 + \left(y_{j_{i+1}} - y_{j_i}\right)^2}. \tag{4}$$

The corresponding number of points on target profile j is $n_j = m_j + 1$.

For a provisional target profile, the piece lengths $s_{j_i} \leq s_d$, as Eq. 3 generates slightly more segments than would exactly match the profile using the piece length s_d. Moreover, any curvature of the design profile results in piece lengths shorter than s_d, as seen in Fig. 2. That is, a piece length $s_{j_i} = s_d$ only when s_d divides exactly into C_j pieces

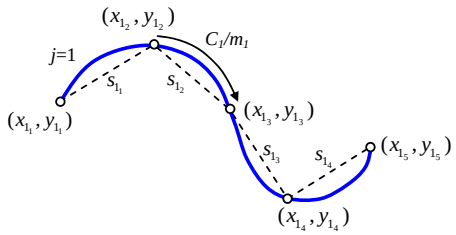

Figure 2: Design profile (solid) with an approximating target profile (dashed) where points are positioned to give a constant arc length along the design profile.

and the design profile has a zero curvature portion long enough to include the entire piece. The average piece length for the j^{th} profile is

$$\bar{s}_j = \frac{1}{m_j}\left(\sum_{i=1}^{n_j-1} s_{j_i}\right). \tag{5}$$

As the provisional target profile is constructed to (potentially) have too many pieces to accurately achieve s_d, the likely scenario is that fewer pieces will produce a value of $\bar{s}_j$ closer to s_d. An error representing the difference between the average segment length and desired segment length is calculated as $\epsilon_{s_j} = \left|s_d - \bar{s}_j\right|$. Decreasing n_j by 1 and redistributing points along the design profile creates a new target profile. Points are removed until $n_j = n_j^*$ (and correspondingly, $m_j = m_j^*$), the number of points minimizes ϵ_{s_j}. The end result is the fewest n_j^* points are used to construct the j^{th} target profile such that all linear piece lengths are approximately equal to the desired segment length. Desirable target profiles are those with the fewest pieces that achieve the accuracy needed to satisfactorily represent the original design profiles. The more pieces used in a set of target profiles, the closer the approximation of the design profiles. Conversely, as the calculations presented in the later sections are dependent on this number, having fewer pieces reduces computation time.

After each m_j^* is established, the total length of the j^{th} target profile is calculated as

$$S_j = \sum_{i=1}^{m_j^*} s_{j_i}. \tag{6}$$

Applying this process to all design profiles, p target profiles are constructed such that all linear pieces have lengths that are approximately equal to s_d. The average length of all m_j^* linear pieces on all p profiles is

$$\bar{s}_m = \frac{\sum_{j=1}^{p} S_j}{\sum_{j=1}^{p} m_j^*}. \tag{7}$$

If the representation of the design profiles lacks the desired accuracy, a smaller desired piece length may be used to increase the number of points defining the target profiles.

Three target profiles are shown in Fig. 3. The lengths of the design profiles are $C_1 = 26.1738$, $C_2 = 31.0847$, and $C_3 = 34.4737$. For a desired piece length of $s_d = 0.35$, the target profiles have $m_1^* = 76$, $m_2^* = 90$, and $m_3^* = 99$ pieces.

The average piece length is $\bar{s}_m = 0.3499$ and the lengths of the target profiles are $S_1 = 26.1669$, $S_2 = 31.0760$, and $S_3 = 34.4562$. Although $S_1/C_1 = 0.9997$, $S_2/C_2 = 0.9997$, and $S_3/C_3 = 0.9995$ in this example, the heuristic in this work is to set s_d such that $S_i/C_i \geq 0.99$ for all profiles in the set unless the design problem dictates a specific accuracy. Values are reported in this initial example to four decimal places to highlight the minor differences between design and target profile lengths and desired and achieved piece lengths. The four decimal places are not meant to indicate these are significant figures.

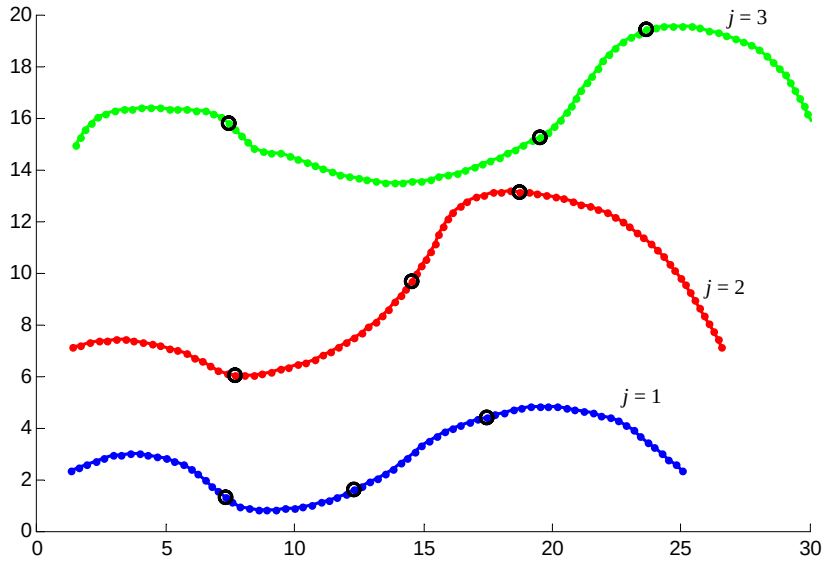

Figure 3: Three design profiles with significantly different arc lengths represented with target profiles of nearly constant piece length.

3. Segmentation

After target profiles with nearly constant piece lengths have been established to adequately represent the design profiles, the rigid bodies that form the edge geometry of the profiles must be created. The segmentation process identifies q portions, or segments, of a target profile that when repositioned will best match the corresponding portions on the other target profiles. An acceptable error in matching profiles is dependent on the application and is at the discretion of the designer.

Mean or $\mathscr{M}$-segments represent a fixed length portion on the set of target profiles, as shown in Fig. 4, and will be embodied by rigid revolute-revolute (RR) links. Constant curvature or $\mathscr{C}$-segments consist of variable length portions on the set of profiles, shown in Fig. 5, and will be embodied by a pair of rigid links forming a revolute-prismatic-revolute (RPR) chain. Once identified, the segments are created and assembled into a chain that can be moved to approximate the full set of design profiles.

When the set of design profiles have similar arc lengths, the chain of rigid-bodies that adequately approximates them may contain all $\mathscr{M}$-segments. For the general case, when the design profiles have significantly different arc lengths, each target profile will have a different number of points since the pieces have roughly equal lengths. The difference in arc length is quantified by the difference in the number of pieces used in defining the target profiles. For appreciable differences, at least one of the segments must be a $\mathscr{C}$-segment. As described in the following sections, the segments are created through an iterative process that reduces shape-approximating error.

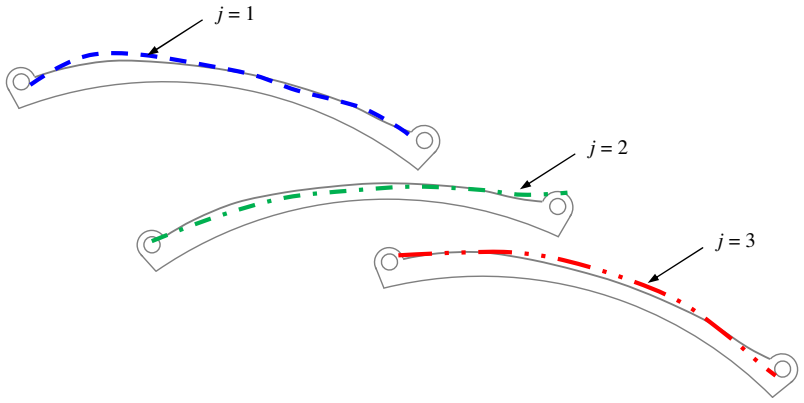

Figure 4: A $\mathscr{M}$-segment represents a single revolute-revolute link that corresponds to groups of equal numbered pieces on each target profile.

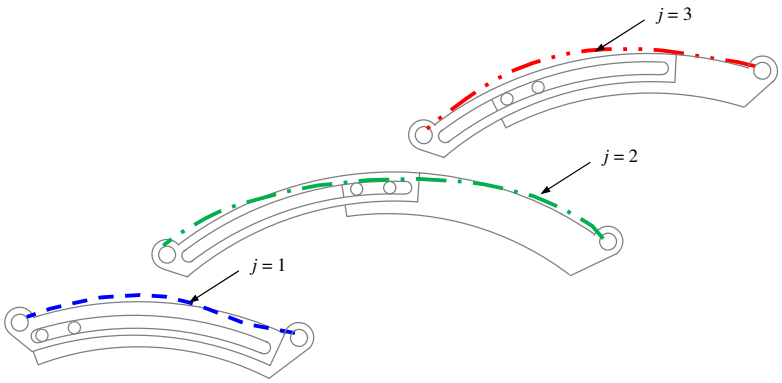

Figure 5: $\mathscr{C}$-segments are variable arc length groups of pieces consisting of a different number of points on each target profile and represent a revolute-prismatic-revolute chain.

3.1. Segments

Certain restrictions are placed on identifying the q groups of points that will form segments on each of the target profiles. The number of pieces on the e^{th} segment of the j^{th} profile is designated m_j^e, and the number of points is

$n_j^e = m_j^e + 1$. Since an $\mathscr{M}$-segment represents a single rigid link, a fundamental constraint on forming $\mathscr{M}$-segments is that the number of pieces in those segments should be constant across all p profiles. That is, if the e^{th} segment is an $\mathscr{M}$-segment, $m_1^e = m_2^e = \ldots = m_p^e$. Since the $\mathscr{C}$-segments are used to compensate for differences in length among the profiles, the number of pieces in corresponding $\mathscr{C}$-segments from different profiles will generally be different. The number of pieces in the $\mathscr{C}$-segments on the j^{th} profile must be selected such that $\sum_{e=1}^{q} m_j^e = m_j^*$.

The points that lie on the boundary between segments are termed segmentation points, which also include the first and last points on the target profile. Points on the j^{th} target profile are numbered 1 through n_j^*. The index of the segmentation point at the start of the e^{th} segment on the j^{th} profile is designated as k_j^e. The index of the final point of that segment is k_j^{e+1}. Note that k_j^{e+1} is also the index of the first point on the $e+1$ segment. Thus,

$$k_j^1 = 1 \qquad j = 1, \ldots, p \tag{8}$$

$$k_j^e = k_j^{e-1} + m_j^{e-1} = 1 + \sum_{i=1}^{e-1} m_j^i \qquad e = 2, \ldots, q \qquad j = 1, \ldots, p \tag{9}$$

$$k_j^{q+1} = n_j^* \qquad j = 1, \ldots, p. \tag{10}$$

The same number of segments q and their types (i.e. $\mathscr{M}$- or $\mathscr{C}$-segments) must be maintained for all profiles. A design vector $\mathbf{V}$ defines the number of segments and their types in a candidate design. As an example, $\mathbf{V} = [\mathscr{M}\ \mathscr{C}\ \mathscr{M}\ \mathscr{C}]$ specifies that four segments ($q = 4$) will be formed, with the first being an $\mathscr{M}$-segment, followed by a $\mathscr{C}$-segment, an $\mathscr{M}$-segment and a $\mathscr{C}$-segment. Currently, an a-priori method to determine the best $\mathbf{V}$ for a set of design profiles is lacking. The designer can specify $\mathbf{V}$ based on intuition after inspecting the shape of the profiles, or the error minimizing process can cycle through several design vectors to attain an adequate fit to the set of target profiles. Any combination of $\mathscr{M}$ or $\mathscr{C}$-segments is possible. For a design with q segments, there are $2^q - 1$ different design vectors that contain at least one $\mathscr{C}$-segment. It is noted that a $\mathscr{C}$-segment represents two rigid links, while an $\mathscr{M}$-segment represents one rigid link in the shape-approximating chain.

3.2. The Segment Matrix

A $p \times q$ segment matrix SM identifies the number of pieces in each segment and is constructed consistent with the design vector. The j^{th} row of SM represents the j^{th} target profile and contains the number of pieces for each segment on that profile. From an implementation standpoint, segments should not be so small that a physical embodiment is impractical. A minimum number of segment pieces α is defined such that $m_j^e \geq \alpha,\ e = 1, \ldots, q,\ j = 1, \ldots, p$.

As an example, consider the set of three target profiles from Fig. 3 having $m_1^* = 76$, $m_2^* = 90$, and $m_3^* = 99$ pieces, respectively. Based on physical constraints, $\alpha = 5$ was specified. With $\mathbf{V} = [\mathscr{M}\ \mathscr{C}\ \mathscr{M}\ \mathscr{C}]$, an initial segment matrix may be constructed as

$$SM_1 = \begin{bmatrix} m_1^1 & m_1^2 & m_1^3 & m_1^4 \\ m_2^1 & m_2^2 & m_2^3 & m_2^4 \\ m_3^1 & m_3^2 & m_3^3 & m_3^4 \end{bmatrix} = \begin{bmatrix} 15 & 13 & 9 & 38 \\ 15 & 9 & 9 & 56 \\ 15 & 39 & 9 & 35 \end{bmatrix}. \tag{11}$$

Since the first segment is an $\mathscr{M}$-segment, the same number of pieces has been selected to be used on all profiles: $m_j^1 = 15$, $j = 1, \ldots, 3$. Similarly for the third segment, $m_j^3 = 9$, $j = 1, \ldots, 3$. Being $\mathscr{C}$-segments, all instances of the second and fourth segments do not need to have the same number of pieces. The number of pieces in the second segment are individually selected. Being the final $\mathscr{C}$-segment in $\mathbf{V}$, the fourth segment will contain all remaining pieces in the profile. That is, $m_1^4 = 38$, such that for $j = 1$, $15 + 13 + 9 + 38 = 76 = m_1^*$, and likewise for the other profiles. The segmentation points can be calculated with Eqs. 8, 9, and 10. For $j = 1$, $k_1^1 = 1$, $k_1^2 = 16$, $k_1^3 = 29$, $k_1^4 = 38$, and $k_1^5 = 76$. The segmentation points are indicated with black circles in Fig. 3.

Once an initial SM is formulated, an iterative process creates the segments, evaluates how well they match the target profiles and adjusts SM to minimize the error. The method for creating the segments is described in the following two sub-sections. The details of the evaluation and adjustment process are explained in Section 4.

3.3. $\mathscr{M}$-Segments

The process of creating an $\mathscr{M}$-segment is identical to that described in Murray et al. [19] and is summarized here for completeness. The process begins by shifting all points on the segment to a common location so a single profile can be generated that approximates the shapes of all segments within the set. The first profile is selected as the common location, so each segment from the second through last profile is shifted to the first profile. Each point on the the e^{th} segment is shifted by a rigid body transformation in the plane,

$$\mathbf{Z}_{j_i}^e = \mathbf{A}_j^e \mathbf{z}_{j_i} + \mathbf{d}_j^e \qquad i = k_j^e, \ldots, k_j^{e+1} \qquad j = 2, \ldots, p, \tag{12}$$

where

$$\mathbf{A}_j^e = \begin{bmatrix} \cos\theta_j^e & -\sin\theta_j^e \\ \sin\theta_j^e & \cos\theta_j^e \end{bmatrix}, \qquad \mathbf{d}_j^e = \begin{bmatrix} x_j^e \\ y_j^e \end{bmatrix}. \tag{13}$$

Although a general solution for the transformation is well-established in the image registration literature [27, 28, 29, 30], Murray et al. [19] developed a closed-form method to determine θ_j^e and $\mathbf{d_j^e}$ such that the sum of the distances between each point on the shifted segments and the corresponding point on the reference segment is minimized. Then, a new piecewise linear curve is constructed where each point is the geometric center of the set of p corresponding points in the shifted segments.

$$\mathbf{Z}_{m_i} = \frac{1}{p}\left(\mathbf{z}_{1_i} + \sum_{j=2}^{p} \mathbf{Z}_{j_i}\right) \qquad i = k_j^e, \ldots, k_j^{e+1}. \tag{14}$$

This new curve becomes the $\mathscr{M}$-segment and represents one rigid RR link in the shape-changing chain. A second minimization process determines a rotation matrix $\hat{\mathbf{A}}_j^e$ and translation $\hat{\mathbf{d}}_j^e$ to shift instances of the mean segment back to profiles 2 through p to approximate the shape of the segment on each target profile.

$$\bar{\mathbf{z}}_{j_i}^e = \left(\hat{\mathbf{A}}_j^e\right)^{-1}\left(\mathbf{Z}_{m_i} - \hat{\mathbf{d}}_j^e\right) \qquad i = k_j^e, \ldots, k_j^{e+1} \qquad j = 2, \ldots, p. \tag{15}$$

The first segments from the three profiles ($e = 1$, $j = 1, 2, 3$) presented in Fig. 3 are shown in Fig. 6a and shifted to distance-minimizing positions relative to the first profile in Fig. 6b. Figure 6c shows the creation of an $\mathscr{M}$-segment that approximates the set, which is shifted back to each target profile in Fig. 6d.

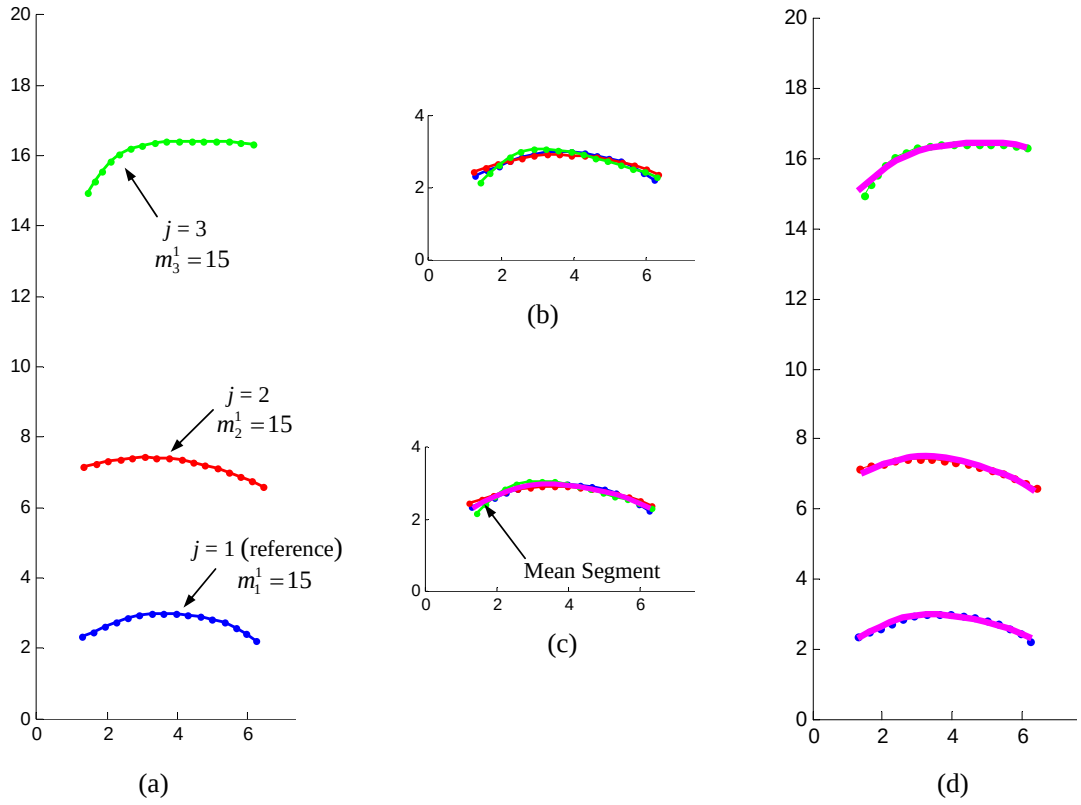

Figure 6: (a) The first segment from three target profiles to be represented by one mean segment. (b) Segments 2 and 3 shifted to reference segment 1 in a distance minimizing transformation. (c) The mean segment is generated as the average of the corresponding segment points. (d) The mean segment is shifted back to the original segments in another distance minimizing transformation.

3.4. $\mathscr{C}$-Segments

A constant curvature $\mathscr{C}$-segment is created using discrete, signed, radius of curvature values at each point along the segment for all target profiles [26]. The radius of curvature value of the j^{th} target profile at the i^{th} point is the radius of an arc r_{j_i} that passes through $\mathbf{z}_{j_i}$ and the neighboring points $\mathbf{z}_{j_{i-1}}$ and $\mathbf{z}_{j_{i+1}}$ [31]. The radius of curvature is computed for each point on the e^{th} segment as

$$r_{j_i} = \frac{\left\|\mathbf{z}_{j_{i+1}} - \mathbf{z}_{j_{i-1}}\right\|}{2\sin\theta} \qquad i = k_j^e + 1 \ldots, k_j^{e+1} - 1 \qquad j = 1, \ldots, p. \tag{16}$$

where θ is the angle $\angle \mathbf{z}_{j_{i-1}} \mathbf{z}_{j_i} \mathbf{z}_{j_{i+1}}$ [32].

A direction vector $\mathbf{P}_{j_i}$ is defined such that it extends from $\mathbf{z}_{j_{i-1}}$ to $\mathbf{z}_{j_i}$.

$$\mathbf{P}_{j_i} = \left\{ \begin{array}{c} x_{j_i} - x_{j_{i-1}} \\ \\ y_{j_i} - y_{j_{i-1}} \end{array} \right\}. \tag{17}$$

If the determinant $\left| \mathbf{P}_{j_i} \quad \mathbf{P}_{j_{i+1}} \right|$ is positive, the radius of curvature is designated positive [33]. The mean radius of the e^{th} segment on all profiles is

$$\bar{r}^e = \frac{1}{\sum_{j=1}^{p} m_j^e - 1} \left(\sum_{j=1}^{p} \left(\sum_{i=k_j^e+1}^{k_j^{e+1}-1} r_{j_i} \right) \right). \tag{18}$$

The curvatures of the first and last points are not included in the average.

Instances of a $\mathscr{C}$-segment are created by generating points $\bar{\mathbf{Z}}_{j_i}^e$ along a radius $\bar{r}^e$ and arc length

$$L_j^e = m_j^e \, \bar{s}^e, \tag{19}$$

where the average length of the pieces on the e^{th} segment on all p profiles is

$$\bar{s}^e = \sum_{j=1}^{p} \left(\frac{1}{m_j^e} \left(\sum_{i=k_j^e+1}^{k_j^{e+1}-1} s_{j_i} \right) \right). \tag{20}$$

As with the $\mathscr{M}$-segments, instances of the $\mathscr{C}$-segment are placed at each target profile in a distance minimizing transformation using Eq. 15.

Each of the second segments from the three profiles ($e = 2$, $j = 1, 2, 3$) presented in Fig. 3 are shown in Fig. 7a with a mean piece length of $\bar{s}_m = 0.35$ and each having a different number of pieces ($m_1^1 = 13$, $m_2^1 = 9$ and $m_3^1 = 39$). A mean radius is calculated as $\bar{r}^1 = 15.06$, and arcs with lengths of $L_1^1 = 4.55$, $L_2^1 = 3.42$ and $L_3^1 = 13.65$ are constructed and fit through the profiles as shown in Fig. 7b.

4. Evaluating and Adjusting the Segment Matrix

Once instances of the segments are created as specified by SM, their shape-approximation errors are evaluated. The maximum point-to-point distance on the j^{th} instance of the e^{th} segment to the corresponding point on the j^{th} profile is

$$E_j^e = \max \left| \bar{\mathbf{z}}_{j_i}^e - \mathbf{z}_{j_i} \right| \qquad i = k_j^e, \ldots, k_j^{e+1}. \tag{21}$$

Similar to SM, a $p \times q$ error matrix EM organizes E_j^e for all segments on all profiles. Error metrics that assist in segment adjustment include the maximum overall error,

$$E_{max} = \max \left(E_j^e \right) \qquad e = 1, \ldots, q \qquad j = 1, \ldots, p, \tag{22}$$

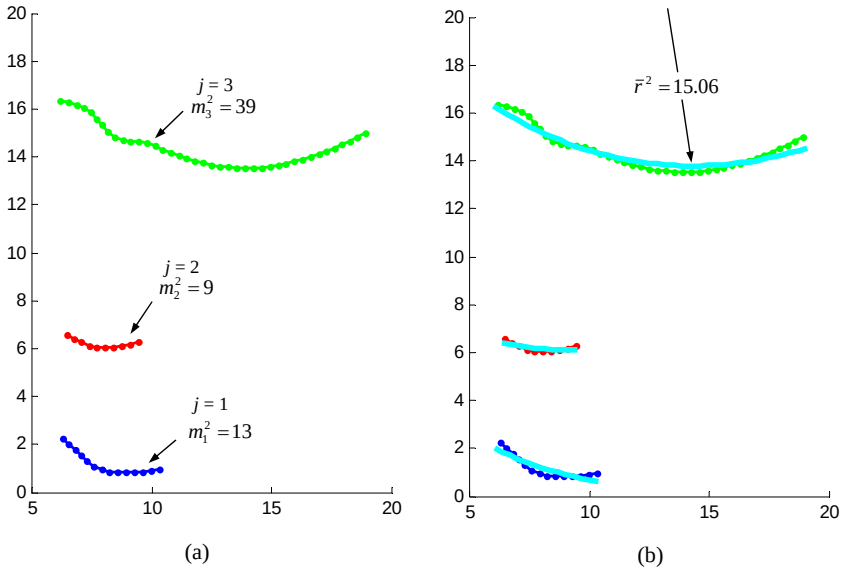

Figure 7: (a) The second segment from three target profiles approximated with a $\mathscr{C}$-segment. (b) An arc of the same radius, but varying length, approximates the segment on all profiles.

the mean error of the e^{th} segment,

$$\bar{E}^e = \sum_{j=1}^{p} E_j^e, \tag{23}$$

and the overall mean error

$$\bar{E} = \frac{1}{q} \sum_{e=1}^{q} \left(\frac{1}{p} \sum_{j=1}^{p} E_j^e \right). \tag{24}$$

An example of the EM that corresponds with the profiles from Fig. 3 and the initial SM of Eq. 11 is

$$EM_1 = \begin{bmatrix} E_1^1 & E_1^2 & E_1^3 & E_1^4 \\ E_2^1 & E_2^2 & E_2^3 & E_2^4 \\ E_3^1 & E_3^2 & E_3^3 & E_3^4 \end{bmatrix} = \begin{bmatrix} 0.10 & 0.32 & 0.04 & 0.43 \\ 0.15 & 0.19 & 0.03 & 1.37 \\ 0.19 & 0.46 & 0.06 & 1.5 \end{bmatrix}. \tag{25}$$

In Eq. 25, $E_{max} = 1.50$ and $\bar{E} = 0.40$. For the $\mathscr{M}$-segments, $\bar{E}^1 = 0.15$ and $\bar{E}^3 = 0.04$.

The number of pieces in each segment can be changed to improve the shape approximation and consequently reduce E_{max}. Adjustments to SM involve either adding, removing or preserving the number of pieces in each segment in order to balance the errors, i.e., E_{max} approaches $\bar{E}$. For a $\mathscr{C}$-segment, each E_j^e is compared to $\bar{E}$. If $E_j^e < \bar{E}$, the segment fits the profile better than the average and can be lengthened to balance the error. A change $\delta m_j^e = +1$ is assigned to that instance of the segment, meaning that one piece will be added. Conversely, if $E_{e_j} > \bar{E}$, that instance of the segment has a below average fit and $\delta m_j^e = -1$ is assigned, meaning that one piece will be removed.

Because all $\mathscr{M}$-segments must be adjusted the same amount, each $\bar{E}^e$ is compared to $\bar{E}$. If $\bar{E}^e < \bar{E}$, a change is assigned to all profiles $\delta m_j^e = +1$, $j = 1, \ldots, p$. Since a segment cannot violate the minimum number of pieces

constraint, a $\delta m_j^e = 0$ may be assigned if $m_j^e = \alpha$. Additionally, the total number of pieces on each profile must remain the same,

$$\sum_{e=1}^{q} \delta m_j^e = 0, \qquad j = 1, \ldots, p. \tag{26}$$

As in the generation of SM, the final $\mathscr{C}$-segment within $\mathbf{V}$ is not adjusted according to its error. Instead, it is adjusted to ensure that the j^{th} profile retains m_j^* pieces. Hence, either no change or changes greater than one may be assigned to the instances of the last $\mathscr{C}$-segment.

The changes are added to SM to obtain an adjusted SM with which a new segmentation trial is conducted. The iterative process continues, assessing errors at each step in order to achieve a final segment matrix with a low point-to-point error. The iterations are stopped when the current value of E_{max} is greater than or equal to the previous five values. To avoid a local minimum, these error-reducing iterations are performed on several initial SM matrices. The SM associated with the lowest value of E_{max} within the entire error history is deemed as the distance minimizing set of segments. These error-reducing iterations were conducted on the four-segment chain of Fig. 3 and the SM of Eq. 11. The segment matrix with the lowest E_{max} is

$$SM_f = \begin{bmatrix} 19 & 12 & 14 & 30 \\ 19 & 22 & 14 & 34 \\ 19 & 42 & 14 & 23 \end{bmatrix}, \tag{27}$$

which resulted in an error matrix

$$EM_f = \begin{bmatrix} 0.17 & 0.22 & 0.33 & 0.17 \\ 0.26 & 0.10 & 0.15 & 0.20 \\ 0.19 & 0.23 & 0.21 & 0.32 \end{bmatrix}. \tag{28}$$

The error metrics were reduced to $E_{max} = 0.33$ and $\bar{E} = 0.22$ (from $E_{max} = 1.50$ and $\bar{E} = 0.40$ with SM_1). The rigid-body chain associated with the initial segmentation is shown in Fig. 8a, whereas Fig. 8b shows the chain after the error-reducing iterations.

5. Joining the Chain

Since the segments are generated individually, the segmentation point on one segment will not coincide with the corresponding segmentation point on the adjoining segment. As shown in Fig. 9a, $\bar{\mathbf{z}}_{j_i}^e \neq \bar{\mathbf{z}}_{j_i}^{e+1}, \ \forall\, i = k_j^e, \ \ e = 2, \ldots, q$ and $j = 1, \ldots, p$. Since the segments will be connected at their endpoints with revolute joints, each segment must be slightly moved from its error-minimizing position to unite the segmentation points. During this process, each profile is treated individually.

Each point on each segment of the j^{th} profile is relocated by

$$\tilde{\mathbf{z}}_{j_i}^e = \tilde{\mathbf{A}}_j^e \bar{\mathbf{z}}_{j_i}^e + \tilde{\mathbf{d}}_j^e, \qquad i = 1, \ldots, n_j^*, \qquad e = 1, \ldots, m_j, \tag{29}$$

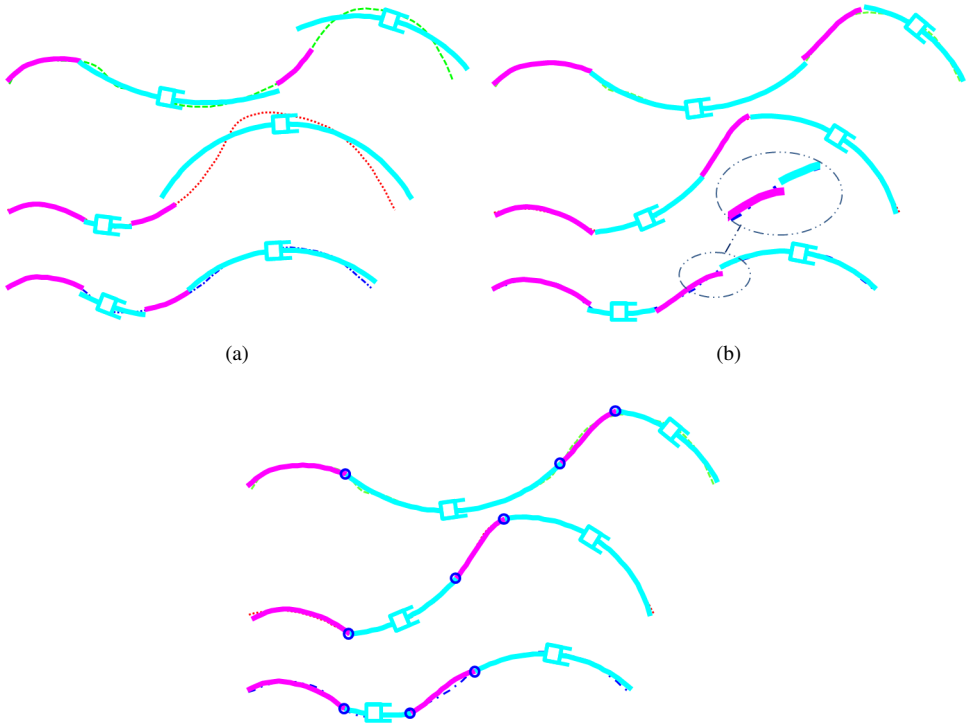

Figure 8: A rigid-body chain that approximates the target profiles. The chain after the initial segmentation matrix is shown in (a) with $E_{max} = 1.50$. The chain after the error-reducing iterations is shown (b) with $E_{max} = 0.33$. The inset illustrates that segmentation points are not coincident. In (c) the joining process unites segmentation points, yet increases the error to $E_{max} = 0.34$.

where

$$\tilde{\mathbf{A}}_j^e = \begin{bmatrix} \cos\tilde{\theta}_j^e & -\sin\tilde{\theta}_j^e \\ \sin\tilde{\theta}_j^e & \cos\tilde{\theta}_j^e \end{bmatrix}, \qquad \tilde{\mathbf{d}}_j^e = \begin{bmatrix} \tilde{x}_j^e \\ \tilde{y}_j^e \end{bmatrix}.$$

The endpoints of adjacent segments must be coincident, which formulates the principal constraint,

$$\tilde{\mathbf{z}}_{j_i}^e = \tilde{\mathbf{z}}_{j_i}^{e+1} = \tilde{\mathbf{z}}_{j_i} \quad \forall \quad i = k_j^e, \quad e = 2, \ldots, q \qquad j = 1, \ldots, p. \tag{30}$$

For closed-loop target profiles, additional constraints include

$$\sum_{e=1}^{q} l_e \cos\tilde{\theta}_j^e = 0, \qquad \sum_{e=1}^{q} l_e \sin\tilde{\theta}_j^e = 0, \qquad j = 1, \ldots, p, \tag{31}$$

where l_e is the length of the line segment connecting the first and last point on segment e. For fixed-end target profiles, additional constraints include

$$\tilde{\mathbf{z}}_{j_1}^1 = \mathbf{z}_{j_1}, \qquad \tilde{\mathbf{z}}_{j_{n_j^*}}^q = \mathbf{z}_{j_{n_j^*}}. \tag{32}$$

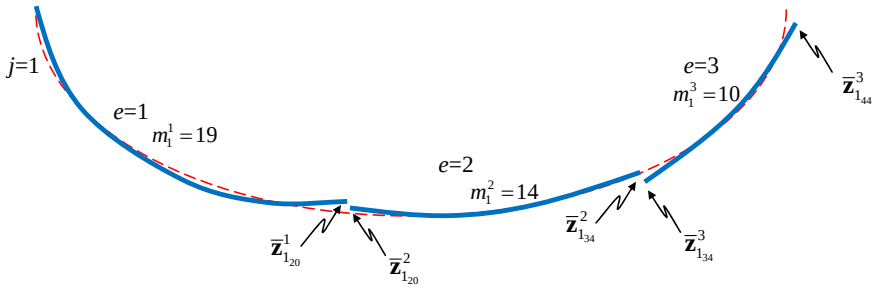

(a) Segmentation points do not coincide

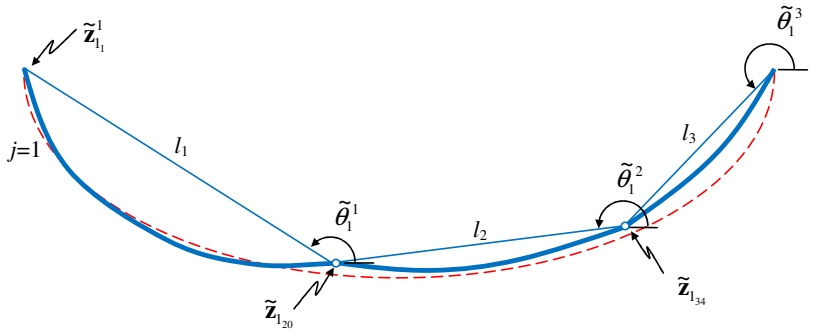

(b) Segments are repositioned to unite segmentation points

Figure 9: After instances of segments are created, the segmentation points will not coincide. To merge the segmentation points and form a chain connected by revolute joints, each segment must be repositioned by adjusting $\tilde{\mathbf{z}}^1_{j_1}$ and $\tilde{\theta}_e$.

As in Persinger et al. [20] the segmentation points are united through a numerical optimization to determine $\tilde{\mathbf{z}}^e_{j_1}$ $e = 2, \ldots, q$ subject to Eq. 30, and if appropriate, 31 or 32. As shown in Fig. 9b, the location of the first point on each j^{th} instance of the chain $\tilde{\mathbf{z}}^1_{j_1}$, the angle of each segment instance $\tilde{\theta}^e_j$, and the translation $\tilde{\mathbf{d}}^e_j$ are the $q+2$ optimization variables. The objective function f to be minimized is the sum of the squared point-to-point distances between points on the instance of the segments and the points on the j^{th} target profile,

$$f = \sum_{i=1}^{k^e_j} \left[\tilde{\mathbf{z}}^e_{j_i} - \mathbf{z}_{j_i}\right]^T \left[\tilde{\mathbf{z}}^e_{j_i} - \mathbf{z}_{j_i}\right] \qquad e = 1, \ldots, q. \tag{33}$$

The *fmincon* function in the optimization toolbox of MATLAB is well suited for this type of constrained nonlinear multivariable problem. The position of the segments as determined by the segmentation process generally serves as a suitable initial guess.

Once optimized, $\tilde{\mathbf{z}}^e_{j_i}$, $e = 2, \ldots, q$, $i = 2, \ldots, n^*_j$ defining the chain of rigid links joined with revolute and prismatic

joints is complete. The optimization is conducted for the other profiles as well, resulting in a rigid-body chain that can be repositioned to approximate all target profiles.

The results of the joining process for the three profiles presented in Fig. 3 is shown in Fig. 8c. After the error-reducing iterations on SM, the maximum point-to-point error was $E_{max} = 0.33$. However, after shifting segments to merge segmentation points, the maximum point-to-point error increased to $E_{max} = 0.34$.

If the accuracy of the approximation is deemed unsatisfactory, the designer can return to the segmentation phase and dictate a different design vector $\mathbf{V}$ or increase the number of segments. To compare alternative designs, the number of joints in the chain of rigid-bodies should be considered. $\mathscr{M}$-segments represent R-R links, so they contain two joints, whereas $\mathscr{C}$-segments represent R-P-R chains and contain 3 joints. Generally, a chain of rigid-bodies with a greater number of joints provides a better approximation to the profiles at the expense of greater mechanical complexity. From a practical perspective of constructing a mechanism, it is desirable to find a compromise between the number of joints and the error between the chain of rigid-bodies and the target profiles.

6. Compound Segment Types

Since the number of links in the chain increases the mechanical complexity, it is desirable to fuse some of the links together when the rotation of a revolute joint is small. To investigate the benefit of each revolute joint in the chain of rigid-bodies, the range of motion is calculated to determine whether the joint is necessary. Recall that $\mathbf{P}_{j_i}$ is the direction vector that extends from $\mathbf{z}_{j_{i-1}}$ to $\mathbf{z}_{j_i}$. Accordingly, the direction vector that extends from the preceding point towards the e^{th} segmentation point on the j^{th} profile is $\mathbf{P}_{j_{k_j^e}}$, and $\mathbf{P}_{j_{k_j^e+1}}$ is the vector from the e^{th} segmentation point to the next point. The relative joint angle at the e^{th} segmentation point is designated as σ_j^e and is represented by the angle from $\mathbf{P}_{j_{k_j^e}}$ to $\mathbf{P}_{j_{k_j^e+1}}$. Thus, the range of motion exhibited by that joint is

$$\Delta\sigma^e = \max\left(\sigma_j^e\right) - \min\left(\sigma_l^e\right) \qquad j = 1, \ldots, p, \qquad l = 1, \ldots, p. \tag{34}$$

If the range of motion is smaller than a specified limit, $\Delta\sigma^e < \sigma_{max}$, the revolute joint motion is considered insignificant during shape approximation. That joint may be considered unnecessary and eliminated to reduce the complexity. If the revolute joint connects two $\mathscr{M}$-segments, the designer is advised to select a new design vector $\mathbf{V}$ with fewer segments. If the revolute joint connects a $\mathscr{C}$-segment with either another $\mathscr{C}$-segment or an $\mathscr{M}$-segment, the joint can be eliminated, clamping the segments at the mean angle. Eliminating the joint creates a compound segment that merges the two original segments. Returning to the example profiles of Fig. 3, the reduced-error chain of Fig. 8 is shown in Fig. 10a. However, the range of motion of the 2^{nd} revolute joint is $\Delta\sigma^e = 12.2°$ and may be considered insignificant. The segments were merged to create the chain shown in Fig. 10b. Eliminating the revolute joint increased the maximum point-to-point error from $E_{max} = 0.34$ to $E_{max} = 0.45$. However, the number of segments and kinematic complexity have been reduced at a modest expense of error.

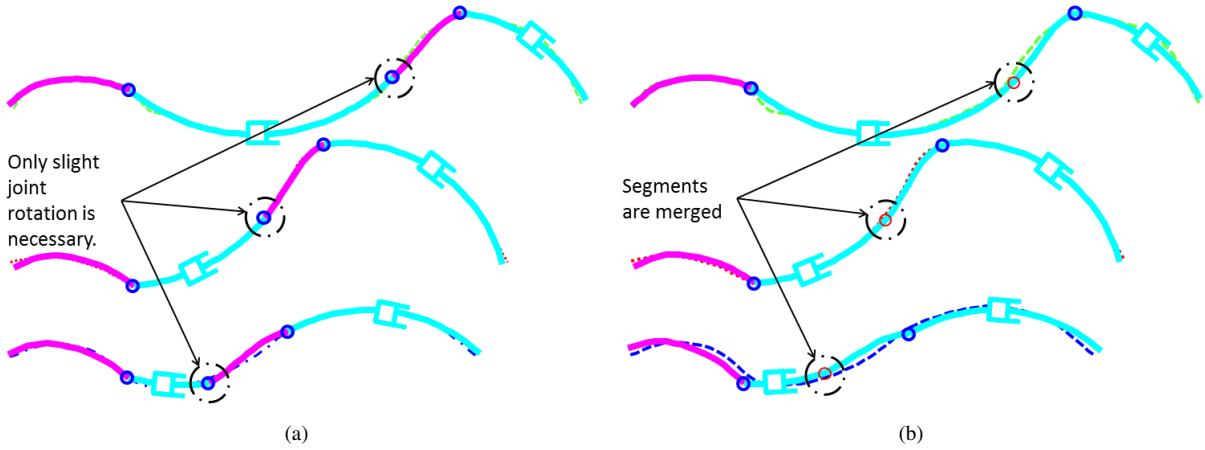

Figure 10: (a) The original chain consisted of 4 segments resulting in $E_{max} = 0.34$, yet one revolute joint exhibited limited motion. (b) The 2^{nd} and 3^{rd} segments were merged into a compound segment, resulting in a three-segment chain with $E_{max} = 0.46$.

7. Mechanization

The mechanization phase involves adding rigid constraining links and joints, forming a mechanism that smoothly transitions the shape approximating chain between the target profiles with a limited number of actuators. In many applications, the reduced cost and control requirements of fewer actuators outweighs the kinematic complexity. When a single-DOF system is desired and the number of target profiles p is less than or equal to five, it is theoretically possible to add binary links without further increasing the profile matching error. The dimensional synthesis task for rigid body guidance identifies appropriate circle points on the rigid links of the shape approximating chain and center points on the frame. Machine theory texts, such as McCarthy [34], provide various methods for dimensional synthesis for rigid body guidance. However, experience shows that eliminating circuit, branch and order defects becomes problematic with $p > 3$. Balli and Chand [35] provide a thorough discussion of solution rectification. Consequently, for two and three profiles, the mechanization of shape-changing linkages has been accomplished by adapting dimensional synthesis techniques to geometric constraint programming (GCP) with a computer-aided design package as in Kinzel et al. [36].

For greater than three profiles, mechanization is performed as outlined in Murray et al. [19, 20]. Least-square approximations such as those developed by Yao and Angeles. [37] can be used to locate circle and center points for each segment. Structural error associated with such approximate motion synthesis methods will further increase shape approximating error. A search algorithm is implemented to examine many circle and center point pairs, designating candidate designs as those that produce an acceptable level of structural error. The candidate designs are then evaluated to determine whether they can be actuated monotonically to perform the shape change without encountering a circuit

or branch defect. Successful designs can be ranked by a quality factor of the designer's choosing. This search approach does not yield optimal designs in any formal sense, but produces a number of viable designs that can be evaluated according to various metrics. Expanding on the search process, Zhao et al. [21] illustrate how genetic algorithms can be used to synthesize planar rigid-body shape-changing mechanisms. Once a successful mechanism has been formed, it may benefit from the addition of a coupler driver to reduce actuator effort and eliminate mechanism defects [38].

8. Examples

8.1. Fixed-End Profiles

Zhao et al. [21] present applications in which the first and last points on each profile of similar length are fixed. The segmentation process for variable length profiles remains intact when fixed ends are required by merely introducing the additional constraint in Eq. 32. As an example, Fig. 11a shows three profiles with a fixed-end requirement. The arc lengths of the profiles are $C_1 = 12.24$, $C_2 = 12.90$, and $C_3 = 14.13$. A desired piece length of $s_d = 0.35$ was specified, producing $m_1^* = 75$, $m_2^* = 89$, and $m_3^* = 98$. A design vector with six segments was selected, $\mathbf{V} = [\mathscr{C}\,\mathscr{M}\,\mathscr{M}\,\mathscr{C}\,\mathscr{M}\,\mathscr{C}]$, and a minimum number of pieces per segment of $\alpha = 8$ was designated. The final shape-approximating rigid-body chain is shown in Fig. 11b, which exhibits a profile matching error of $E_{max} = 0.18$.

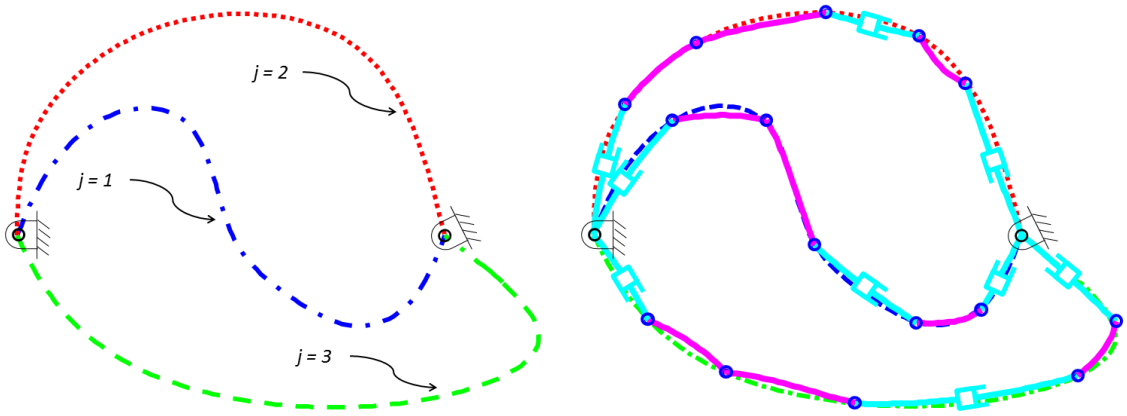

Figure 11: Fixed-end profiles shown in (a). The final, rigid-body, shape-approximating chain is shown in (b) having $E_{max} = 0.18$.

8.2. Automotive Driver's Seat

To illustrate the complete shape-change synthesis process, consider an automotive seat that should comfortably conform to the full range of driver sizes. According to Frey and Tecklin [39], about 80% of American adults suffer from pain in the lumbar spine during their lifetime. Musculoskeletal disorders can be caused by long periods of

driving, the use of manual or stick shift transmissions, and the lack of adequate car seat adjustment [40]. Substantial research in human factors of seat or chair design can be found in the literature [41]. Extensive human measurements at different ages can be found in [42]. These studies can be utilized to define an automotive seat profile that can be adjusted to satisfy the seating requirements for most drivers.

In the design of a seat profile, Fig. 12a shows three drivers seated relative to the steering wheel. The first profile ($j = 1$) conforms to a female from the 1^{st} percentile group. The second profile ($j = 2$) refers to the 99^{th} percentile male group. A mid-range profile is inserted to ensure that a middle profile is achieved corresponding with average-sized drivers and to produce a smooth transition between the two extreme driver sizes. Accordingly, an intermediate profile ($j = 3$) is created from the 50^{th} percentile male group. The three design profiles shown in Fig. 12b are identified with significantly different lengths of both the seat and the back rest portions. These profiles have arc lengths of $C_1 = 44.42$, $C_2 = 51.98$ and $C_3 = 54.39$. A desired piece length is set as $s_d = 0.35$, generating target profiles having $m_1^* = 127$, $m_2^* = 149$, $m_3^* = 155$ pieces.

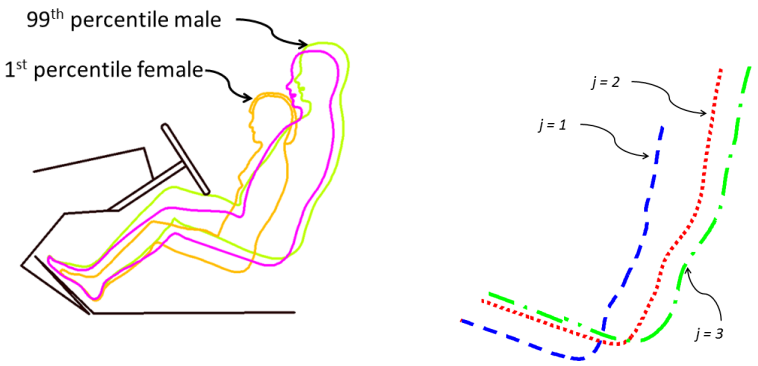

(a) Drivers at the steering wheel (b) Design profiles for seat

Figure 12: (a) The silhouettes of a small, an average and a large driver [42]. (b) Seat design profiles that ideally suit the small, average and large drivers from (a).

A five-segment seat was specified for the segmentation process. A search through every possible five-segment design vector was performed, with $\mathbf{V} = [\mathscr{C}\ \mathscr{M}\ \mathscr{M}\ \mathscr{M}\ \mathscr{C}]$ producing the lowest error approximation. Figure 13 presents the results from the segmentation process yielding $E_{max} = 0.27$. Further, two revolute joints exhibited minimal rotation. They were eliminated, creating a compound segment within the chain as shown in Fig. 13b, yielding $E_{max} = 0.50$.

Using the mechanization methods described in Section 6, links were added to reduce the DOF and form a mechanism that is able to alter its shape between the three profiles in Figs. 14. Incorporating prismatic joints, Fig. 14 shows the final single-DOF mechanism that moves between the three profiles to suit the small, average, and large drivers.

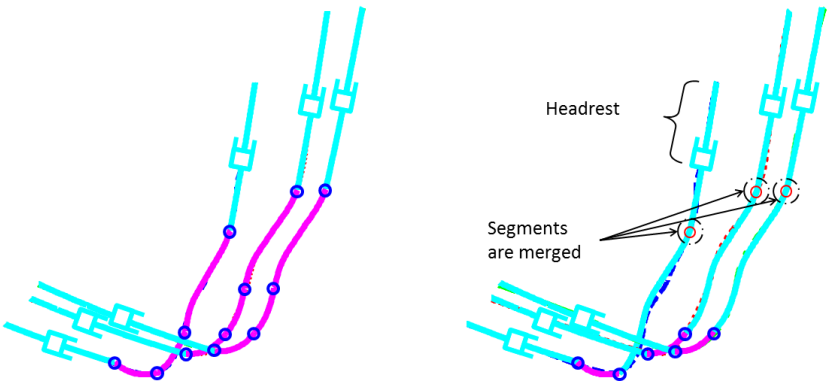

(a) Optimized design with E_{max} = 0.2736

(b) Optimized design with reduced number of segments, E_{max} = 0.4988

Figure 13: The three seat profiles can be approximated by the five segment shape-approximating chain in (a). The creation of a compound segment reduces the chain to three segments in (b) with only a modest increase in error.

9. Conclusion

A planar serial chain of rigid bodies connected by revolute and prismatic joints can be reconfigured to approximate any number of curves. A necessary step in the design of rigid-body shape-changing mechanisms is to determine the planar chain that best matches a set of curves, called design profiles. This paper presents the theory and a practical methodology for defining the shapes of the rigid bodies and identifying the proper sequence of revolute and prismatic joints to connect them in order to minimize the error between the chain and the design profiles. In service of this process, the design profiles are converted to target profiles, curves by which neighboring points are approximately the same distance apart. Contiguous sets of points may be compared among target profiles to identify both the ideal geometry for the rigid bodies comprising the chain as well as the joint locations and types. Several examples display the utility of the described procedures.

Acknowledgment

This material is based upon work supported by the National Science Foundation under Grants #1234374 and #1234383. Additionally, the first author would like to thank the Ministry of Higher Education of Malaysia for sponsoring his studies and research at the University of Dayton.

References

[1] A. Y. N. Sofla, S. A. Meguid, K. T. Tan, W. K. Yeo, Shape morphing of aircraft wing: Status and challenges, Material Design 31(3) (2010) 1284-1292.

[2] S. Vasista, L. Tong, K.C. Wong, Realization of morphing wings: A multidisciplinary challenge, Journal of Aircraft 49(1) (2012) 11-28.

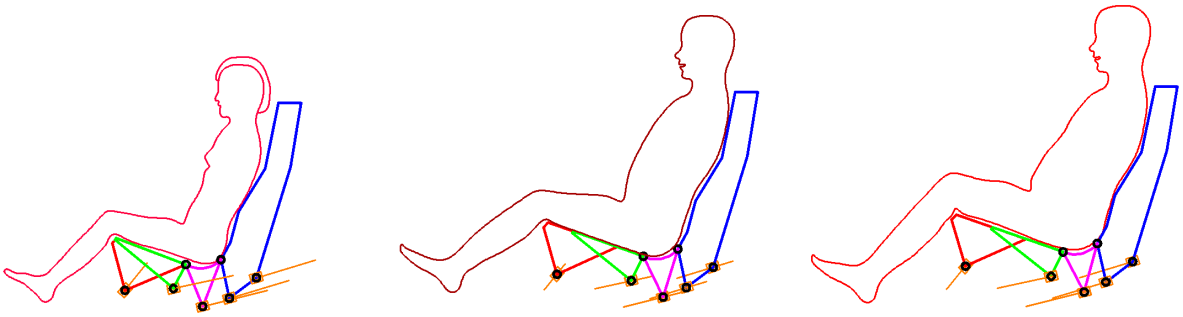

(a) Position 1 (b) Position 2 (c) Position 3

Figure 14: The results of the mechanization process: (a) The seat is adjusted for the small woman. (b) The seat accommodating the medium man. (c) The car seat is positioned for the large person.

[3] G. J. Frank, J. J. Joo, B. P. Sanders, D. M. Garner, A. P. Murray, Mechanization of a high aspect ratio wing for aerodynamic control, Journal of Intelligent Material Systems and Structures 19(9) (2008) 1101-1112.

[4] D. Inoyama, B. P. Sanders, J. J. Joo, Topology optimization approach for the determination of the multiple-configuration morphing wing structure, Journal of Aircraft 45(6) (2008) 1853-1862.

[5] S. Kota, J. Hetrick, R. Osborn Design and application of compliant mechanisms for morphing aircraft structures, in: Proc. of the SPIE 5054, Smart Structures and Materials Conference, San Diego, CA, USA, 2003, pp. 24-33.

[6] J. D. Anderson, Fundamentals of Aerodynamics, McGraw-Hill, New York, 2012.

[7] J. T. Wong, Shape morphing structures via intercalation compounds, M.Eng. Thesis, Massachusetts Institute of Technology, 2007.

[8] G. N. Washington, Smart aperture antennas, Smart Materials and Structures 5(6) (1996) 801-805.

[9] J. W. Martin, J. A. Main, G. C. Nelson, Shape control of deployable membrane mirrors, in: Proc. of the ASME Adaptive Structures and Materials Systems Conference, Anaheim, CA, USA, 1998, pp. 217-223.

[10] U. Heselhaus, W. Richter, Folding roof for a convertible, U.S. Patent Number 6,270,143 B1, 2001.

[11] A. G. Erdman, G. N. Sandor, S. Kota, Mechanism Design: Analysis and Synthesis, Vol. 1, 4^{th} ed., Prentice-Hall, New York, 2001.

[12] S. Hirose, Y. Umetani, The development of soft gripper for the versatile robot hand, Mechanism and Machine Theory 13(3) (1978) 351-359.

[13] M. Kato, S. Sano, Y. Hiyoski, Variable section extrusion die set and variable extrusion molding method, U.S. Patent Number 3,526,020, 1996.

[14] M. D. Murphy, A. Midha, L. L. Howell, The topological synthesis of compliant mechanisms, Mechanism and Machine Theory 31(2) (1996) 185-199.

[15] K. J. Lu, S. Kota, Design of compliant mechanisms for morphing structural shapes, Journal of Intelligent Material Systems and Structures 14(3) (2003) 379-391.

[16] Y. M. Moon, Bio-mimetic design of finger mechanism with contact aided compliant mechanism, Mechanism and Machine Theory 42(5) (2007) 600-611.

[17] P. Limaye, G. Ramu, S. Pamulapati, G. K. Anathasuresh, A compliant mechanism kit with flexible beams and connectors along with analysis and optimal synthesis procedures, Mechanism and Machine Theory 49(3) (2012) 21-39.

[18] P. R. Lawson, J. L. Yen, A piecewise deformable subreflector for compensation of Cassegrain main reflector errors, IEEE Transactions on Antennas and Propagation 36(10) (1988) 1343-1350.

[19] A. P. Murray, J. P. Schmiedeler, B. M. Korte, Kinematic synthesis of planar, shape-changing rigid-body mechanisms, Journal of Mechanical Design 130(3) (2008) 032302-1-10.

[20] J. A. Persinger, J. P. Schmiedeler, A. P. Murray, Synthesis of planar-rigid-body mechanisms approximating shape changes defined by closed

curves, Journal of Mechanical Design 131(7) (2009) 071006-1-7.

[21] K. Zhao, J. P. Schmiedeler, A. P. Murray, Design of planar, shape-changing, rigid-body mechanisms for morphing aircraft wings, Journal of Mechanisms and Robotics 4(4) (2012) 041007-1-10.

[22] M. N. Mohd Zubir, B. Shirinzadeh, Y. Tian, A new design of piezoelectric driven compliant-based microgripper for micromanipulation, Mechanism and Machine Theory 44(12) (2009) 2248-2264.

[23] T. Huang, H. T. Liu, D. G. Chetwynd, Generalized Jacobian analysis of lower mobility manipulators, Mechanism and Machine Theory 46(6) (2011) 831-844.

[24] H. Ding, F. Hou, A. Kecskeméthy, Z. Huang, Synthesis of the whole family of planar 1-DOF kinematic chains and creation of their atlas database, Mechanism and Machine Theory 47(1) (2012) 1-15.

[25] J. A. Horst, I. Beichl, Efficient piecewise linear approximation of space curves using chord and arc length, Proc. of the SME Applied Machine Vision Conference, Cincinnati, OH, USA, 1996, Vol. 2, pp. 744-747.

[26] F. Mokhtarian, A. K. Mackworth, Theory of multi-scale, curvature-based shape representation for planar curves, IEEE Transactions on Pattern Analysis and Machine Intelligence 14(8) (1993) 789-805.

[27] K. S. Arun, T. S. Huang, S. D. Blostein, Least-squares fitting of two 3-D point sets, IEEE Transactions on Pattern Analysis and Machine Intelligence 9(5) (1987) 698-700.

[28] S. Umeyama, Least-squares estimation of transformation parameter between two point patterns, IEEE Transactions on Pattern Analysis and Machine Intelligence 13(4) (1991) 376-380.

[29] B. K. P. Horn, Closed-form solution of absolute orientation using unit quaternions, Journal of the Optical Society of America 4(4) (1987) 629-642.

[30] B. Zitová, J. Flusser, Image registration methods: A survey, Image and Vision Computing 21(11) (2003) 977-1000.

[31] H. G. Burchard, Discrete curves and curvature constraints, in: Curves and Surfaces in Geometric Design, P. J. Laurent et al. (Eds.), A. K. Peters Ltd., Natick, MA, 1994, pp. 67-74.

[32] S. Stahl, Introduction to Topology and Geometry, John Wiley, Hoboken, NJ, 2005.

[33] D. G. Zill, M. R. Cullen, Advanced Engineering Mathematics, Jones & Bartlett Publishers, Sudbury, MA, 2006.

[34] M. J. McCarthy, Geometric Design of Linkages, Springer-Verlag, New York, 2000.

[35] S.S. Balli, S. Chand, Defects in link mechanisms and solution rectification, Mechanism and Machine Theory 37(9) (2002) 851-876.

[36] E. C. Kinzel, J. P. Schmiedeler, G. R. Pennock, Kinematic synthesis for finitely separated positions using geometric constraint Programming, Journal of Mechanical Design 128(5) (2006) 1070-1079.

[37] J. Yao, J. Angeles, Computation of all optimum dyads in the approximate synthesis of planar linkages for rigid-body guidance, Mechanism and Machine Theory 35(8) (2000) 1065-1078.

[38] D. A. Perkins, A. P. Murray, Singularity free revolute-prismatic-revolute and spherical-prismatic-spherical chains for articulating planar and spherical single degree of freedom mechanisms, Journal of Mechanisms and Robotics 4(1) (2012) 011007-1-6.

[39] J. K. Frey, J. S. Tecklin, Comparison of lumbar curves when sitting on the Westnofa Balans® multi-chair, sitting on a conventional chair, and standing, Physical Therapy 66 (1986) 1365-1369.

[40] P. T. McCabe, Contemporary Ergonomics 2004, CRC Press, Boca Raton, FL, 2004.

[41] S. Pheasant, Bodyspace: Anthropometry, Ergonomics, and the Design of Work, 2^{nd} ed., Taylor & Francis, London, UK, 1996.

[42] A. R. Tilley, The Measure of Man and Woman, Revised ed., John Wiley & Sons, New York, NY, 2002.